ACS NANO
Cite This: ACS Nano XXXX, XXX, XXX–XXX
www.acsnano.org

ARTICLE

Artificial Optoelectronic Synapses Based on Ferroelectric Field-Effect Enabled 2D Transition Metal Dichalcogenide Memristive Transistors

Zheng-Dong Luo,*[,†] Xue Xia,[†] Ming-Min Yang,[†] Neil R. Wilson,[†] Alexei Gruverman,[‡] and Marin Alexe*[,†]

[†]Department of Physics, The University of Warwick, Coventry CV4 7AL, United Kingdom
[‡]Department of Physics and Astronomy, University of Nebraska, Lincoln, Nebraska 68588, United States

Supporting Information

ABSTRACT: Neuromorphic visual sensory and memory systems, which can perceive, process, and memorize optical information, represent core technology for artificial intelligence and robotics with autonomous navigation. An optoelectronic synapse with an elegant integration of biometric optical sensing and synaptic learning functions can be a fundamental element for the hardware-implementation of such systems. Here, we report a class of ferroelectric field-effect memristive transistors made of a two-dimensional WS_2 semiconductor atop a ferroelectric $PbZr_{0.2}Ti_{0.8}O_3$ (PZT) thin film for optoelectronic synaptic devices. The WS_2 channel exhibits voltage- and light-controllable memristive switching, dependent on the optically and electrically tunable ferroelectric domain patterns in the underlying PZT layer. These devices consequently show the emulation of optically driven synaptic functionalities including both short- and long-term plasticity as well as the implementation of brainlike learning rules. Integration of these rich synaptic functionalities into one single artificial optoelectronic device could allow the development of future neuromorphic electronics capable of optical information sensing and learning.

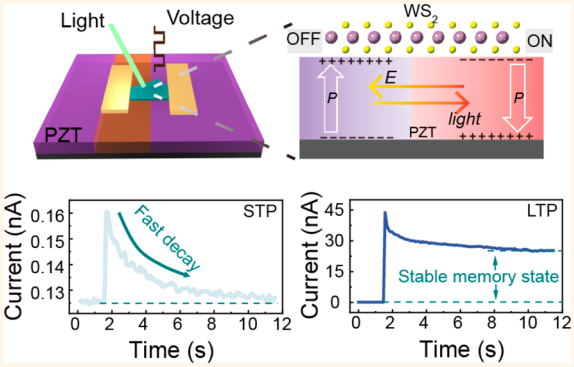

KEYWORDS: *two-dimensional material, ferroelectric, memristive transistor, ferroelectric memory, optoelectronic device*

Emulation of biological visual and learning functions has emerged as a highly sought-after concept in artificial intelligence and neuromorphic electronics for next-generation artificial visual systems.[1−7] Current neuromorphic vision technology is suffering from high circuitry complexity and power consumption, low efficiency, and difficulties in device miniaturization mainly due to the physical separation of the optic sensing, processing and memory units.[1−7] Overcoming these limitations could be achieved by adopting sensory and computation concepts inspired by biology, which demands a more elegant strategy to organize photoreceptors and memory/processing elements. In a real visual memory system,[8] the optical information sensed by the eyes transfers from neuron to neuron through synapses and is processed or "memorized" in neural networks. This "learning" process is enabled by the synaptic plasticity, that is, reconfiguration of connections (or weights) of a synapse caused by the light-induced neural activity. Depending on the strength of the synaptic connection change, two types of synaptic plasticity have been proposed to synergistically complete the ability of "learning" in neural networks:[9−11] short-term plasticity manifesting a temporal synaptic connection variation and long-term plasticity induced by a stronger connection change of the synapse. Therefore, for realizing advanced artificial visual devices with intrinsic optic sensory and neuromorphic computing behaviors, the hardware implementation of a biology-inspired optoelectronic synapse that includes both light detection and emulation of synaptic plasticity learning rules is critical.

Memristors, or memristive devices,[12−15] exhibiting resistive switching (RS) behavior reminiscent of synaptic plasticity in biological synapses, are establishing promising paradigms for artificial neuromorphic electronics.[16,17] However, imitation of

Received: September 28, 2019
Accepted: December 30, 2019
Published: December 30, 2019

Downloaded via UNIV OF NEBRASKA LINCOLN on January 21, 2020 at 23:50:10 (UTC).
See https://pubs.acs.org/sharingguidelines for options on how to legitimately share published articles.

© XXXX American Chemical Society

DOI: 10.1021/acsnano.9b07687
ACS Nano XXXX, XXX, XXX–XXX

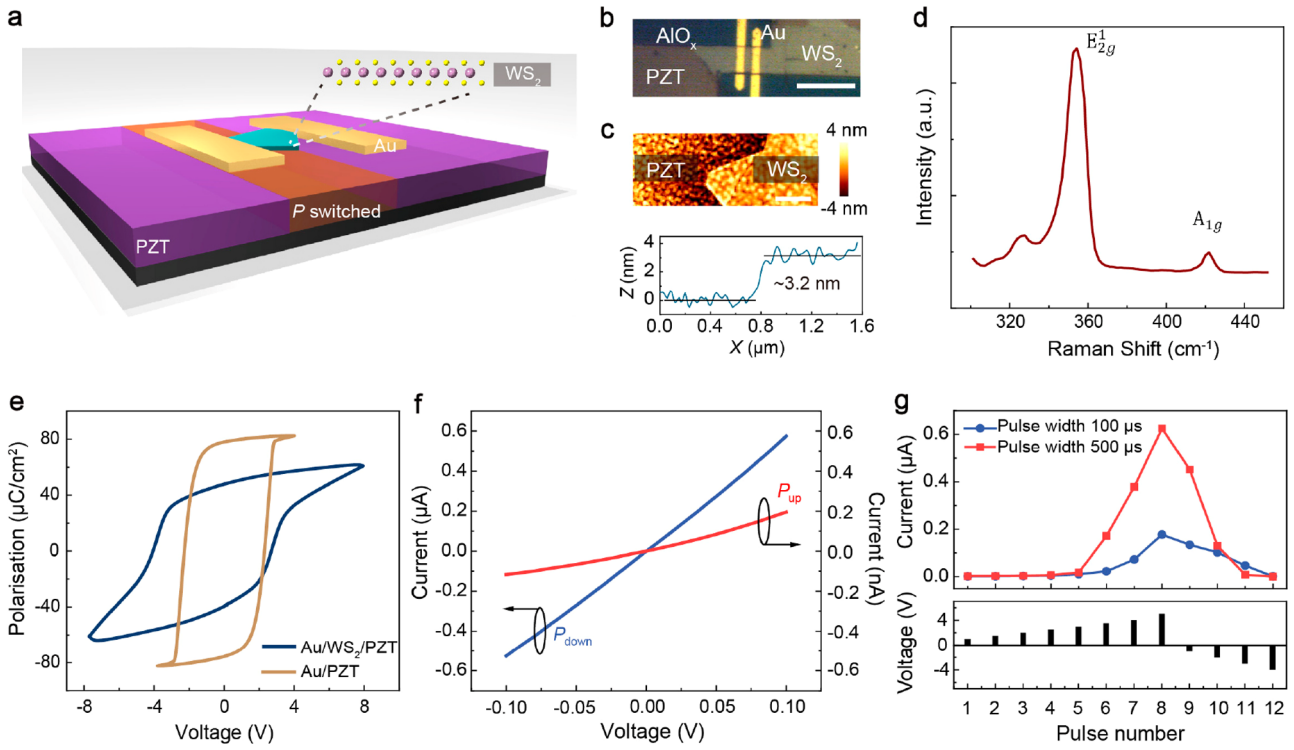

Figure 1. Device configuration and electrical characteristics of the WS_2/PZT FeFET. (a) Schematic drawing of the device geometry. (b) Optical image of a representative WS_2/PZT FeFET device. Scale bar: 20 μm. (c) Topography image and height profile of the WS_2/PZT taken using contact-mode AFM scanning. Scale bar: 1 μm. (d) Raman spectrum of the WS_2 flake used for the device. (e) Ferroelectric hysteresis loops of the same PZT film with Au and Au/WS_2 top electrodes, acquired at 100 Hz voltage frequency. (f) Current−voltage curves of the WS_2 at down and up polarization states of the PZT, respectively. (g) Electrically controlled conductance states of the device with 100 μs (blue) and 500 μs (red) pulses, respectively, where the device readout bias was kept at 0.1 V. The current states were readout after ~1 min waiting time following each voltage pulse.

synaptic responses and human brainlike memory functions through dynamic manipulation of electronic properties in a memristive device, is normally achieved only by using electric stimuli.[18−22] Reliance solely on the electric tunability presents a serious challenge for the application of memristive devices in neuromorphic vision systems since an optoelectronic synaptic device demands the efficient integration of both light and electrical control over the device properties. Therefore, the strong photonic-electronic coupling in a single device is a prerequisite for an optoelectronic memristive synapse.[3,4,23] Unfortunately, for those mainstream memristive elements, *i.e.*, memristors with a two-terminal vertical structure, such a requirement demands the coexistence of electro- and photo-active functionalities in a single RS material, which could be a daunting challenge.

In contrast, the emerging three-terminal transistor-geometry memristive devices appear to be a promising platform to accommodate versatile control parameters and thus increase device functionalities.[24] In such devices, the synergy between the lateral channel material and the neighboring gate component could be exploited to combine distinct physical properties of different elements assembled in one single structure. Atomically thin and transferrable two-dimensional (2D) layered materials, whose physical properties can be strongly influenced by the neighboring substrate or capping layer,[25] are considered as appealing candidates for use as conducting channels in such devices. There has been a plethora of demonstrations of the feasibility of such approach including but not limited to substrate strain induced change of the 2D channel electronic and structural properties,[26] gate dielectric doping enabled modulation of the electronic,[27−29] ferromagnetic[30,31] and photonic behavior,[32,33] ferroelectric-gating nonvolatile switching of transport properties,[34−36] *etc.* However, a pure gate-controllable 2D memristive transistor with simultaneous optical and electrical control, which could address the urgent need for optoelectronic neural synaptic devices, has not yet been demonstrated.

In this work, we report a proof-of-concept demonstration of a class of 2D optoelectronic synapses based on ferroelectric field-effect memristive transistors using a layered transition metal dichalcogenide (TMDC) channel atop a ferroelectric oxide thin film. Here, we use a few-layer-thin WS_2, a typical 2D TMDC semiconductor with excellent optoelectronic properties,[37,38] as a conducting channel and $PbZr_{0.2}Ti_{0.8}O_3$ (PZT) thin film as the ferroelectric gate dielectric whose switchable and permanent polarization can tailor the transport properties in the WS_2 channel.[34−36] Beyond the conventional memristive switching of WS_2 *via* electrical tuning of the PZT polarization, we demonstrate that the WS_2/PZT memristive transistor can emulate complex light-controlled neuromorphic synaptic functionalities, such as short-term plasticity, long-term plasticity and implement the optical information-driven long- and short-term memory learning rules. The presented optoelectronic 2D memristive transistors with complex synaptic functionalities could offer a promising solution for future neuromorphic visual synaptic devices and optoelectronic memory applications.

DOI: 10.1021/acsnano.9b07687
ACS Nano XXXX, XXX, XXX−XXX

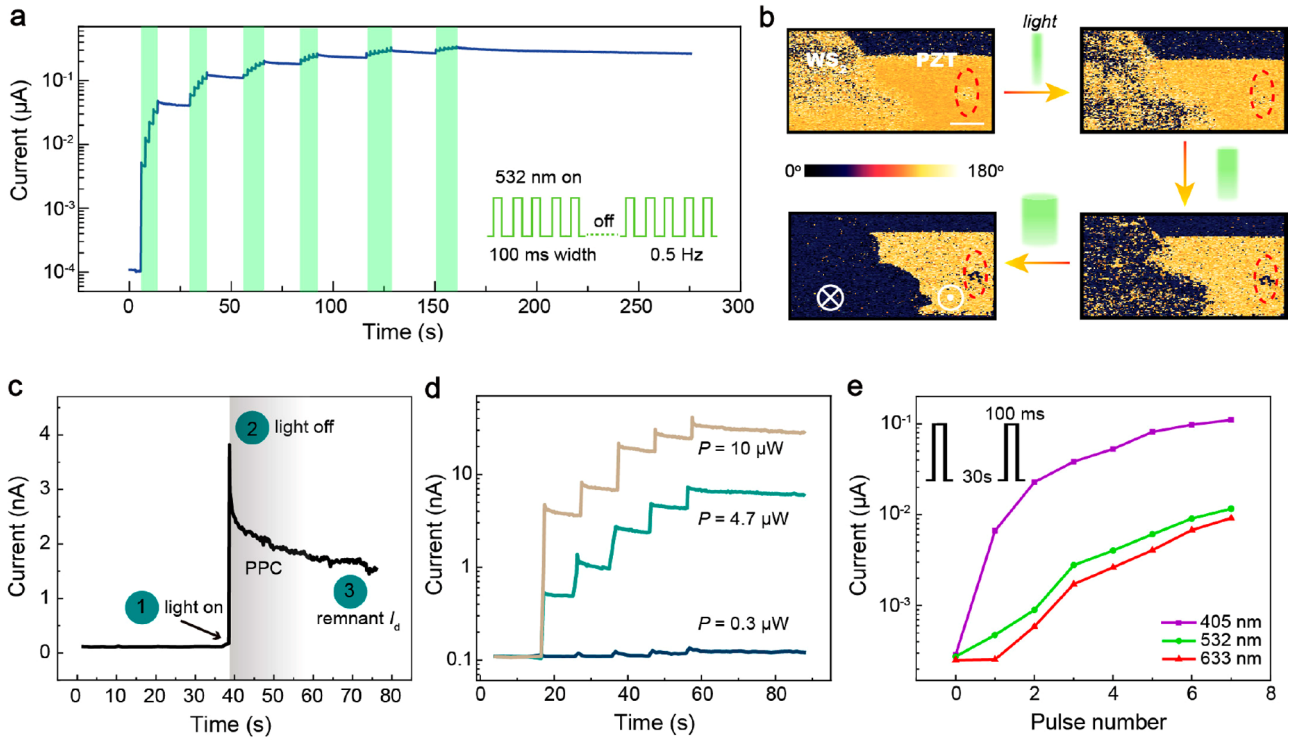

Figure 2. Light programming of memristive levels in WS_2/PZT transistors. (a) Channel conductance evolution by illuminating the WS_2/PZT with 532 nm light pulses. Here, a pulse train consists of five light pulses. (b) PFM images showing the light-induced PZT ferroelectric domain evolution as a function of light exposure time. The red circle highlights the area covered by a small WS_2 flake. Scale bar: 1 μm. (c) Dynamic conductance change of the device after exposed to a single 532 nm light pulse. Light power using 532 nm wavelength (d) and light wavelength (e) dependence of the light-induced conductance switching in WS_2/PZT memristive transistors.

RESULTS AND DISCUSSION

The hybrid WS_2/PZT memristive ferroelectric field-effect transistor (FeFET) is schematically illustrated in Figure 1a. High-quality PZT (~100 nm) thin films were fabricated on ~5 nm $SrRuO_3$ (SRO) conducting layer buffered $SrTiO_3$ (STO) substrates (see the Experimental Section and Figure S1, Supporting Information). WS_2 flakes were obtained from bulk single crystals using the gold-assisted mechanical exfoliation method and then transferred onto those PZT films.[39,40] Au (~200 nm) drain and source electrodes were deposited on the WS_2/PZT heterostructures, defining a 9 μm wide and 2.7 μm long channel; see Figure 1b. In order to minimize the leakage current of the devices, an ~100 nm Al_2O_3 insulating layer was deposited on the sample prior to the electrode fabrication to separate Au electrodes from the PZT layer. The detailed device fabrication process is shown in Figure S2 (Supporting Information). The morphology of the resultant WS_2/PZT heterostructure was checked by atomic force microscopy (AFM). As shown in Figure 1c, the ~3.2 nm thin WS_2 flake was conformally attached to the PZT surface as evidenced by the high resemblance in WS_2 and PZT topography. The WS_2 flake was further analyzed by the Raman spectroscopy, with 532 nm excitation, which confirms the quality of the transferred WS_2; see Figure 1d and Figure S5 (Supporting Information).

Next, we examined ferroelectric properties of the Au/PZT/SRO and Au/WS_2/PZT/SRO capacitor structures, respectively. As shown in Figure 1e, an excellent ferroelectric response was observed in the Au/PZT/SRO capacitor. In contrast, the Au/WS_2/PZT/SRO capacitor showed a robust ferroelectric hysteresis loop but with slightly smaller remnant polarization and asymmetric coercive voltage. We argue that such a change of the ferroelectric hysteresis loop is a manifestation of the ferroelectric polarization induced doping effect in WS_2. As the upward and downward polarizations of PZT introduce massive charge accumulation and depletion in the WS_2, the carrier density variation in the semiconducting WS_2 can greatly change the compensation level to the PZT polarization and thus leads to the observed ferroelectric response difference between Au/WS_2/PZT and Au/PZT structures. Similar results have also been observed in graphene/PZT capacitors.[41]

This ferroelectric polarization doping induced manipulation of WS_2 electronic properties is further confirmed by measuring transport properties of the WS_2/PZT FeFET. As shown in Figure 1f, a distinct conductance change of the WS_2 channel was observed when the PZT polarization directions were fully switched using 1 ms long positive and negative 5 V gate voltage (V_g) pulses. More specifically, the drain currents (I_d) of ~0.6 μA and ~0.2 nA were obtained in WS_2 for polarization down and up states, respectively, at driving voltage V_d = 0.1 V. We also measured the leakage current between the WS_2 channel and gate and found a negligible value (~0.01 nA) at the same readout voltage; see Figure S6 (Supporting Information). Note that in the following results the drain current was readout using a driving voltage of 0.1 V (V_d = 0.1 V) unless otherwise stated. We further investigated the channel conductance modulation as a function of amplitude and duration of applied voltage pulses. Figure 1g shows gradual conductance changes of the WS_2 channel triggered by voltage pulses of varying polarity, amplitude, and duration. This conductance switching features several key characteristics of a memristive device, such as

DOI: 10.1021/acsnano.9b07687
ACS Nano XXXX, XXX, XXX−XXX

nonvolatile and multiple states and frequency dependence,[16] unambiguously proving that the WS_2/PZT FeFET can be operated as a memristive transistor. Here, as observed in ferroelectric-based devices,[34,42,43] the memristive switching is proposed to be due to the voltage history-dependent gradual evolution of up/down ferroelectric domains.[42,43] Specifically, by applying suitable voltages through the WS_2 on the underneath PZT, the PZT could exhibit a series of mixed domain states, namely the coexistence of upward and downward ferroelectric domains underneath the WS_2 channel. The up/down ferroelectric domains giving surface areas with positive or negative polarizations, can result in charge accumulation or depletion in the adjacent WS_2. Therefore, by setting the PZT underneath the WS_2 into different mixed domain states, *i.e.*, different ratios between up and down ferroelectric domains, the WS_2/PZT devices can consequently exhibit various conductance states due to the ferroelectric field effect.

It has been shown previously that in the 2D TMDC/ferroelectric oxide film heterostructure light can switch the ferroelectric polarization.[44] Here, having demonstrated electrically driven memristive properties in the WS_2/PZT FeFET, we now show light-enabled memristive switching in the device. Under periodic exposure of 100 ms long 532 nm light pulses (with the power P = 10 μW at a repetition rate of 0.5 Hz), a dynamic light-programmed conductance switching was observed in the WS_2/PZT FeFET; see Figure 2a. Starting from the insulating state (I_d = ~ 0.1 nA, set by −5 V pulse), with an increasing number of light-pulse trains (each with 5 pulses), the conductance of the WS_2 channel was increased and eventually reached a saturated state with I_d = ~ 0.3 μA which is comparable to the conductance state set by the positive voltage shown in Figure 1g. It is worth noting that the I_d of the WS_2 measured in the dark after each light pulse train shows a long retention, which suggests the great potential of WS_2/PZT FeFET devices for use as multilevel optoelectronic memories.[45]

To explore the underlying mechanism for the light induced conductance switching, we conducted photo-assisted piezoresponse force microscopy (ph-PFM) measurements on WS_2/PZT devices (see Figure S7 in the Supporting Information for the experimental setup). The results are summarized in Figure 2b. We first set the WS_2-covered PZT and part of the bare PZT into the upward polarization state by scanning using 5 V sample bias. Next, we scanned the same area of the WS_2/PZT in the dark after a series of 10 s long light illumination (532 nm, P = ~4 μW). Four representative PFM images obtained during this process are shown here (Figure 2b): with increasing accumulated illumination time, the polarization of the PZT underneath the WS_2 was gradually switched into the downward state, resulting in various mixed domain patterns, while that of the bare PZT kept the same direction. In contrast, the WS_2/PZT with the downward polarization at start showed no change of PFM signal after light illumination. This light-driven ferroelectric polarization switching process can be explained using a recently proposed theory considering the interplay between photoinduced charges in 2D semiconductors and polarization charges in the ferroelectrics.[44] The WS_2/PZT structure has a preferred downward polarization (Figure 1f) and thus a downward build-in electric field (E_{bi}). While the PZT is in an upward polarization state, light-absorption created intralayer excitons in WS_2 decay into interlayer excitons, resulting in positive charge accumulation at the WS_2/PZT interface. These light-induced charges screen the upward polarization and lead to the polarization reversal driven by E_{bi}. Meanwhile, a light-induced polarization switching from downward to upward is not permitted because of the downward-oriented E_{bi}.[44] These results shown in Figure 2b accord well with the light-induced WS_2 conductance change in the device as shown in Figure 2a. These multilevel conductance states after each light pulse trains shown in Figure 2a can thus be attributed to mixed PZT domain states with different ratios between upward and downward ferroelectric domains, which is similar to the electrically controlled memristive switching demonstrated in the previous section.

Detailed analysis of the dynamics of the light-induced conductance change is shown in Figure 2c. After a single 100 ms long light pulse (532 nm, P = 10 μW) on the WS_2/PZT FeFET, a current surge occurred immediately as the consequence of light-induced WS_2 photoconductivity enhancement. Afterward, the conductance of the device reached a stable value (remnant I_d) in responding to the PZT domain rearrangement after a short relaxation process. The optical tuning of the remnant conductance of the WS_2 can be attributed to the light-reconfigured domain state of the PZT. In this case, a higher ratio of downward polarization was created by the light induced switching from the upward polarization state. The relaxation of the conductance can be accounted on the persistent photoconductivity (PPC) in WS_2,[46] which is a widely observed phenomenon in 2D TMDCs (see also Figure S9, Supporting Information). According to the model regarding the light-induced polarization switching in 2D TMDC/ferroelectric heterostructures, the light absorption of WS_2 which affects the charge accumulation at the interface is an important parameter to control the switching process.[44] We verified this idea by detecting the conductance change of the WS_2/PZT device after exposure to light with varying powers and wavelengths. Figure 2d shows increased light-enhanced conductance response in WS_2 with increasing light power. The light pulses used here were with 532 nm wavelength, 100 ms duration, and 0.1 Hz. As can be seen here, by increasing the light intensity from 0.3 to 10 μW, significant conductance enhancement was observed after 5 pulses of light, which suggests that the higher charge accumulation due to stronger light adsorption of WS_2 can indeed lead to a faster polarization switching process in the PZT. WS_2 exhibits higher responsivity to light with shorter wavelength,[47] which suggests that light with higher photon energy could induce stronger charge accumulation at the WS_2/PZT interface and consequently lead to faster polarization switching in PZT. As shown in Figure 2e, by decreasing the light wavelength from 633 to 405 nm, almost 1 order of magnitude change of WS_2 conductance enhancement was observed after same numbers of (7 pulses) of light exposure, proving that light with higher responsivity in WS_2 can cause stronger charge accumulation at the interface. The 633, 532, and 405 nm light with 5.2, 4.7, and 3.9 μW intensities were used here, respectively. Note that the light intensity used for each wavelength was not the same due to experimental limitation. Overall, the light-triggered multilevel and nonvolatile conductance states, and light spectrum response, shown by these WS_2/PZT memristive transistors, indicate their promising potential for emulation of optoelectronic synaptic functions with light color recognition.

Following investigations of electrically and optically tunable memristive switching in WS_2/PZT transistors, we further show

DOI: 10.1021/acsnano.9b07687
ACS Nano XXXX, XXX, XXX−XXX

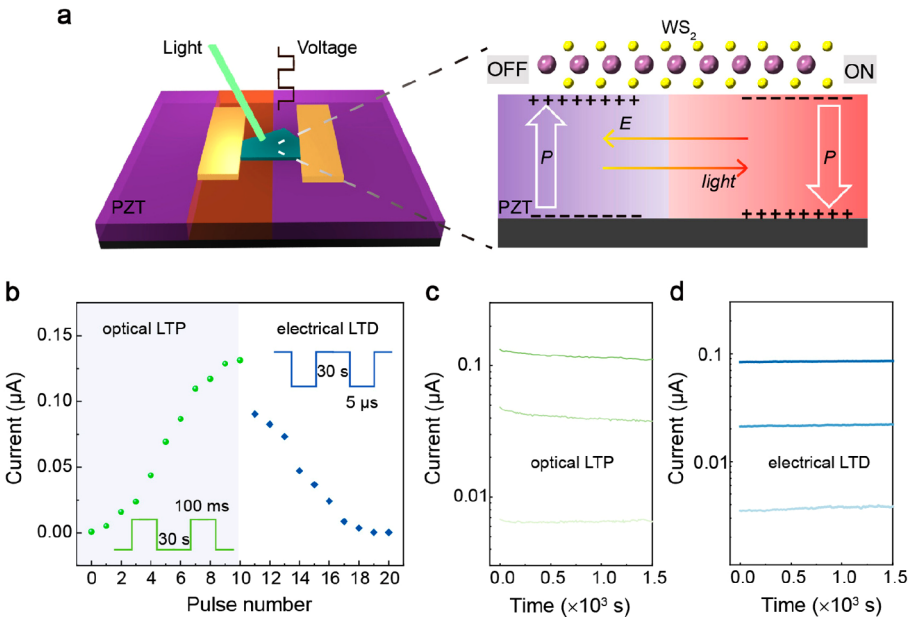

Figure 3. Long-term optical and electrical synaptic plasticity characteristics. (a) Schematic configuration of the device and the mechanism behind the optically and electrically tunable channel conductance. (b) Long-term optical potentiation and electrical depression in the WS_2/PZT optoelectronic synapses. Each current state was taken after 30 s waiting time allowing for the sufficient relaxation following applied light and electrical pulses. Time dependent multilevel conductance states demonstrating memory retention properties of the device during optical LTP (c) and electrical LTD (d) process, respectively.

the realization of three-terminal optoelectronic neural synapses that emulate optical sensing and synaptic plasticity behaviors using WS_2/PZT devices. The basic operating mechanism is shown in Figure 3a. As demonstrated in previous sections, light and voltage can both manipulate mixed ferroelectric domain states in the WS_2 channel covered PZT. Using suitable optical and electrical pulses, the ratio between upward (S_{up}) and downward (S_{down}) domains, *i.e.*, $S_{up}/(S_{up}+ S_{down})$, where $0 \leq S \leq 1$, can be driven into a large number of values between 0 and 1, leading to multilevel conductance values between OFF (lowest conductance) and ON (highest conductance) states in WS_2 channel through the ferroelectric field effect (see Figure 3a). In our memristive transistors, such ferroelectric domain reconfiguration related nonvolatile optical induced conductance increase and electrically induced conductance decrease behaviors can mimic the optically induced long-term potentiation (LTP) and electrically enabled long-term depression (LTD) functions in biologic synapses; see Figure 3b. As illustrated in Figure 3b, the conductance of the WS_2 channel, which can be referred to postsynaptic current (PSC) in a synaptic device, is shown to increase with applying a series of 100 ms long light pulses (532 nm, $P = 10$ μW) and decrease with the repetition of 5 μs long voltage pulses at −3.5 V. The retention characteristics of the device after optical and electrical stimuli are displayed in parts c and d, respectively, of Figure 3. Here, three representative time-dependent PSC decay curves at different current levels taken during optical LTP and electrical LTD process are displayed, clearly demonstrating the stability of the WS_2/PZT optoelectronic synapse against time and further confirms the optoelectrical long-term plasticity synaptic functions.

In neurology, long-term plasticity and short-term plasticity are believed to cooperatively complete learning and memory functionalities in the human brain, that is, long-term memory (LTM) and short-term memory (STM).[11,48] In neuromorphic synaptic devices, while long-term plasticity refers to the ability of holding the memory state for a relatively long time, the short-term plasticity requires the device to relax back to the original conductance state on time scales from milliseconds to minutes after exposure to the external stimuli.[11,22,48,49] In previous studies, ferroelectric-based memristive devices have demonstrated the long-term plasticity synaptic function and its characteristic features like spike-timing-dependent plasticity by exploiting the dynamic ferroelectric domain evolution and robust domain stability.[42,43] However, most of them fail to emulate the short-term plasticity as such a function requires a *volatile* behavior which is against the nature of nonvolatile ferroelectric switching.[18] In the following, different from the long-term plasticity demonstrated above, we show that WS_2/PZT memristive transistor can also exhibit optically induced short-term plasticity using relatively low intensity light excitations.

As shown in Figure 4a, the light-induced conductance enhancement in WS_2 rapidly decays to 0 within 10 s after illumination with a single 0.19 μW and 100 ms long 532 nm light pulse, demonstrating a light-induced short-term potentiation (STP) behavior. In stark contrast, using a higher light intensity (28 μW), a stable enhanced conductance state after the same decay time as that of STP can be observed in Figure 4b. This much slower decay marked by such a retention enhancement agreed well with the LTP behavior. To better analyze memory retention (M_t), we define M_t as the normalized time dependent current decay[48]

$$M_t = (I_t - I_{off})/(I_{max} - I_{off}) \quad (1)$$

where I_t is the current changing with time, I_{off} is the initial current, and I_{max} is the maximum current. The relaxation behavior of light induced memory state change can then be described by the Kohlrausch stretched-exponential function[22,48,49]

$$M_t \sim \exp[-(t/\tau)^{\beta}] \quad (2)$$

DOI: 10.1021/acsnano.9b07687
ACS Nano XXXX, XXX, XXX−XXX

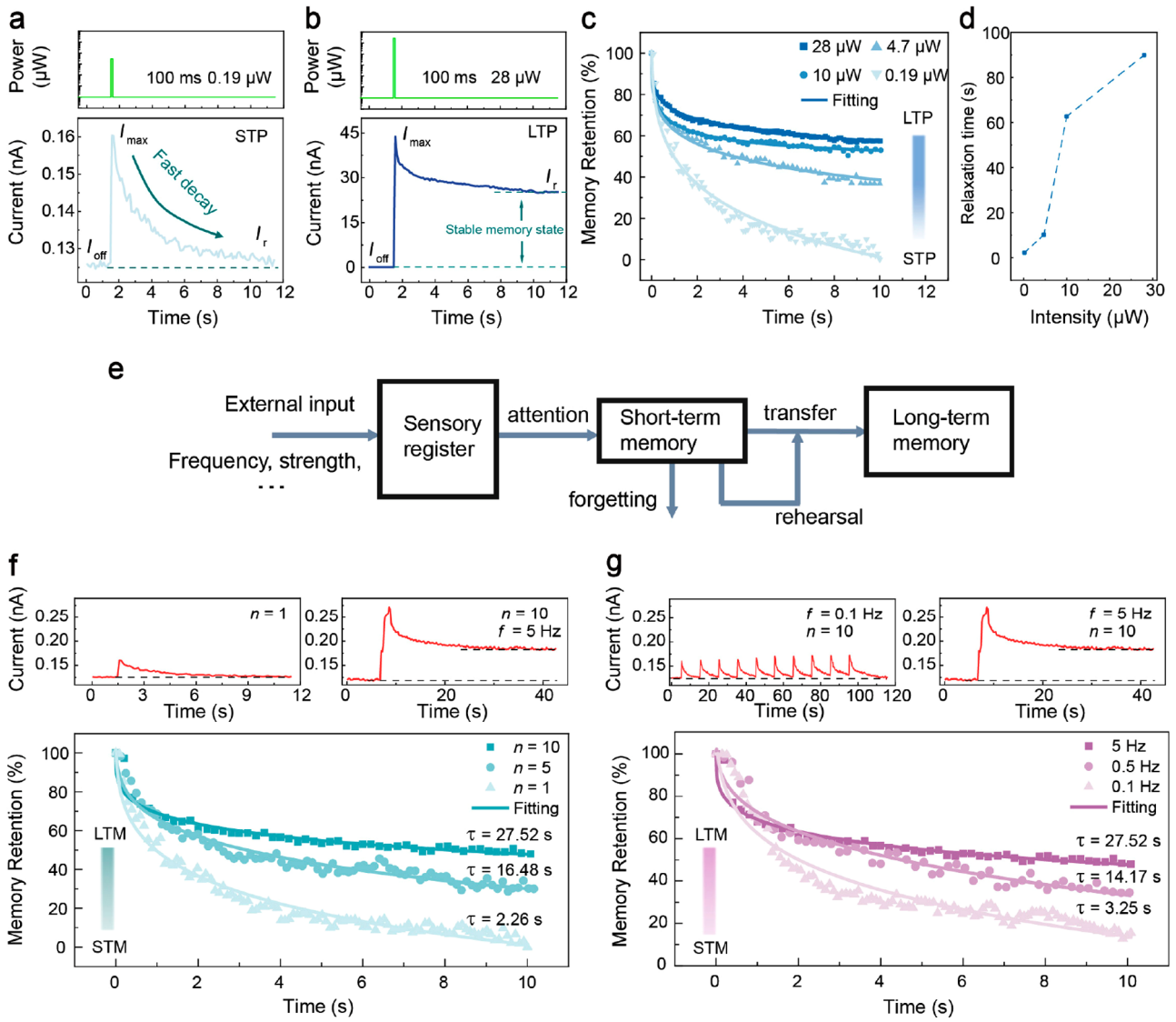

Figure 4. Optical visual memory emulation characteristics. Optical input triggered STP (a) and LTP (b) behaviors by intensity varied light illumination. Evolution of memory retention behaviors (c) and corresponding relaxation time (d) with varying intensities of input light. Line for eye guidance only in (d). (e) Schematic drawing of a psychological human brain memory model, *i.e.*, the multistore model. STM and LTM performance mimicked by the optoelectronic synapse and the transition between STM and LTM by controlling the number (f) and frequency (g) of applied 532 nm light pulses (100 ms duration, P = 0.19 μW).

where τ is the characteristic relaxation time and β is the stretch index ranging between 0 and 1. On termination of a single light pulse excitation, the device memory retention in STP mode (Figure 4a) rapidly decreased with time and remained as only 0.05% after 10 s, with relaxation time τ = 2.26 s. In contrast, within the same period after light illumination, the device kept a relatively high memory retention (~58%) in LTP mode despite a fast initial-stage decline (Figure 4b), with a significantly improved relaxation time τ = 89.92 s. Here, the volatile light response of the STP can be attributed to the PPC effect in WS_2: the low-intensity light used in Figure 4a was not sufficient to induce a permanent or large amount PZT domain change, which would have given a corresponding nonvolatile conductance modulation in WS_2 (Figure 4b), but was strong enough to cause a photoconductivity enhancement of the WS_2 which experienced a fast decay after the input light was removed (STP).

We further studied the light intensity dependent memory retention properties of WS_2/PZT optoelectronic synapses; the results are summarized in Figure 4c,d. With increasing light intensity, a STP to LTP transition can be clearly observed through the enhanced memory retention (Figure 4c). The light intensity dependent characteristic relaxation time obtained from fitting using eq 2 is plotted in Figure 4d. A nearly 45-fold increase in relaxation time is observed by increasing the light intensity from 0.19 to 28 μW. This obvious improvement of relaxation time with increasing light intensity agrees well with the STP-LTP transition, demonstrating the resemblance between memory retention of the presented memristive transistors and that of biological memory systems, *i.e.*, fast decay in short-term plasticity and slower change in long-term plasticity. Overall, the demonstrated coexistence of such volatile and nonvolatile conductance switching unlocks the possibility of emulating the light-induced short-term and long-term synaptic behaviors using the optoelectronic memristive

DOI: 10.1021/acsnano.9b07687
ACS Nano XXXX, XXX, XXX−XXX

transistor, essential for mimicking brain-like learning and memory rules.

Leveraging on the combined short-term and long-term plasticity functionalities in our memristive devices, emulation of the biological visual memory functions following a well-known psychological model of human memory, "the multistore model", was performed.[11] The "multistore model" is shown in Figure 4e and can be briefly summarized as newly received information in the sensory register is selectively transferred to the short-term store, in which the information (STM) undergoes a "forgetting" process and can generally be retained only for a short time; With rehearsal, the STM can then be transformed to a LTM in the long term store which can be maintained for a significantly longer time despite the presence of natural "forgetting".[11,49] The optically controlled STP, LTP, and their transition as demonstrated in our memristive devices are in congruence with this psychological memory model. Below we show the emulation of loss and strengthening effects of the visual memory as well as their transition behaviors using our optoelectronic memristive transistors. For the STM-LTM emulation, similar to reported electronic neuromorphic devices wherein subthreshold external stimuli are often adopted,[48,50,51] we used relatively low intensity light pulse (532 nm, 100 ms duration, P = 0.19 μW) as the optical stimulus. A single excitation using the subthreshold/low-intensity stimulus normally is not sufficient to cause a permanent change of the device memory state, but repetition of the applied stimuli (as in rehearsal of the "multistore model") can gradually trigger a longer-lasting memory state change (LTM). In the WS_2/PZT optoelectronic memristive transistor, we show that the memory loss and strengthening effect can be tuned by applied light pulse number and frequency, manifesting the emulated STM-LTM transition by "rehearsal". Here, as in previous analysis of light-induced STP, the memory loss is due to volatile potentiation by the PPC effect of WS_2, while the long-term remnant enhancement of memory can be attributed to the light accumulation induced stable ferroelectric domain reconfiguration in PZT. As shown in Figure 4f,g, with increasing the number and frequency of the light pulses, a gradual low to high PSC amplitude change and enhancement of memory retention in the WS_2/PZT memristive transistor can be observed. In Figure 4f, by increasing the number (n) of identical 100 ms-long light pulses from 1 to 10 under the same frequency (5 Hz), the device shows an enhanced memory retention with ~14-fold increase of characteristic relaxation time. An alternative approach to emulating the STM-LTM behavior can be achieved by changing the frequency of the applied light pulses, *i.e.*, the interval between two successive pulses. With increasing the frequency (f) of applied 10 pulses of 100 ms long light from 0.1 to 5 Hz, the device exhibits a transition from fast-decay and low-amplitude current change to slow-relaxation conductance enhancement as shown in Figure 4g. The observed great improvement of relaxation time with repetition of applied light pulses (rehearsal) thus suggests that the presented WS_2/PZT memristive transistor can efficiently emulate STM, LTM, and their transition as in the human memory system. Overall, optical short-term and long-term plasticity triggered by increasing light intensity, pulse numbers and frequency are emulated using the WS_2/PZT optoelectronic memristive transistor, suggesting that the presented artificial synapse has attained the ability to mimic complex optical information triggered biological learning functionalities.

CONCLUSIONS

In summary, we have fabricated WS_2/PZT optoelectronic memristive transistors that can simultaneously respond to optical and electrical stimuli to emulate biological optical sensing and synaptic functions at the same time. In particular, the memristive devices exhibit both volatile and nonvolatile light-induced conductance switching that correlate to optically controllable short-term and long-term plasticity dynamics. These working patterns, as required for an optoelectronic synapse, can be selected by varying the intensity, wavelength, duration, and number of input light pulses. Moreover, the optically controllable PSC change in our devices could enable the implementation of a psychology human memory model beyond the pure emulation of biological synaptic behaviors. This research presents a promising platform for accommodating both biometric optical sensing and synaptic functionalities in a simple structure, could contribute to the hardware implementation of future optoelectronic synaptic neural networks.

EXPERIMENTAL SECTION

Device Fabrication. PZT/SRO/STO thin films were prepared by depositing ~100 nm PZT and ~5 nm SRO epitaxial thin films on (001)-oriented STO substrates using pulsed laser deposition (PLD). The SRO layer was first grown at 680 °C with the oxygen partial pressure at 0.15 mbar followed by the PZT layer deposition at 600 °C and 0.2 mbar of oxygen partial pressure. During the film growth, a KrF excimer laser at power density of 0.83 J cm^{-2} and repetition rate of 7 Hz was used. WS_2 flakes were obtained by exfoliation from the single crystals using the Scotch tape method and transferred onto the PZT films. Field-effect transistors on selected WS_2 flakes were fabricated with Al_2O_3 buffer layers and Au electrodes using standard photolithography process (AZ5214 photoresist), e-beam evaporation, and lift-off. A detailed description of WS_2 transfer and field-effect transistor fabrication is schematically presented in the Supporting Information; see Figure S2.

Characterization of the Devices. Structural information on PZT/SRO films was collected by high-resolution X-ray diffraction (HR-XRD) using a Panalytical X'pert Pro diffractometer. Raman spectra from WS_2 flakes were obtained using a Renishaw inVia Reflex Raman Microscope with 532 nm excitation. AFM and PFM images were acquired through the XE-100 park AFM system using the NSC 14/Pt (Mikromasch) cantilever. A detailed configuration of the light-assisted PFM measurement can be found in the Supporting Information, Figure S7. Ferroelectric hysteresis loops of the devices were recorded using an aixACCT TF3000 ferroelectric workstation. Conductance states of WS_2/PZT field-effect transistors were measured using a Keithley 2635 electrometer, while a Tektronix AFG 3102 function generator was used to apply voltage pulses. All of the laser diodes were purchased from Thorlabs, and their illumination intensity was checked using a calibrated Newport 818-UV-L silicon photodiode. Applied light pulses were generated using a HP 8116A function generator. WS_2/PZT field-effect transistors were placed in a vacuum probe station at pressure of ~1×10^{-6} mbar during electrical characterizations; see Figure S8 (Supporting Information).

ASSOCIATED CONTENT

Supporting Information

The Supporting Information is available free of charge at https://pubs.acs.org/doi/10.1021/acsnano.9b07687.

Structural and ferroelectric properties of PZT films; WS_2 exfoliation and transistor fabrication process; Effect of vacuum annealing on WS_2/PZT/SRO structures; Raman investigations of transferred WS_2 flakes; Leakage current measurements of WS_2/PZT/SRO structures;

DOI: 10.1021/acsnano.9b07687
ACS Nano XXXX, XXX, XXX−XXX

Experimental setups for measurements; PPC effect in a WS_2/PZT heterostructure; Optical STP and LTP behaviors of WS_2/PZT transistors; Electrical LTP and LTD behaviors of WS_2/PZT transistors (Supplementary Notes 1−9) (PDF)

AUTHOR INFORMATION

Corresponding Authors

*Email: luozhengdong7@gmail.com.
*Email: M.Alexe@warwick.ac.uk.

ORCID

Zheng-Dong Luo: 0000-0003-3725-4912
Neil R. Wilson: 0000-0002-2592-3077
Alexei Gruverman: 0000-0003-0492-2750
Marin Alexe: 0000-0002-0386-3026

Notes

The authors declare no competing financial interest.

ACKNOWLEDGMENTS

Z.D.L. acknowledges the University of Warwick for the Chancellor's International Scholarship. M.A. acknowledges the Wolfson Research Merit and Theo Murphy Blue-sky Awards of Royal Society. This work was partly supported by the EPSRC (UK) through Grant Nos. EP/M022706/1, EP/P031544/1, and EP/P025803/1.

REFERENCES

(1) Indiveri, G.; Douglas, R. Neuromorphic Vision Sensors. *Science* **2000**, *288*, 1189−1190.
(2) Koch, C.; Mathur, B. Neuromorphic Vision Chips. *IEEE Spectrum* **1996**, *33*, 38−46.
(3) Chen, S.; Lou, Z.; Chen, D.; Shen, G. An Artificial Flexible Visual Memory System Based on an UV-Motivated Memristor. *Adv. Mater.* **2018**, *30*, 1705400.
(4) Gao, S.; Liu, G.; Yang, H.; Hu, C.; Chen, Q.; Gong, G.; Xue, W.; Yi, X.; Shang, J.; Li, R. W. An Oxide Schottky Junction Artificial Optoelectronic Synapse. *ACS Nano* **2019**, *13*, 2634−2642.
(5) Seo, S.; Jo, S. H.; Kim, S.; Shim, J.; Oh, S.; Kim, J. H.; Heo, K.; Choi, J. W.; Choi, C.; Oh, S.; Kuzum, D.; Wong, H. P.; Park, J. H. Artificial Optic-Neural Synapse for Colored and Color-Mixed Pattern Recognition. *Nat. Commun.* **2018**, *9*, 5106.
(6) Sun, J.; Oh, S.; Choi, Y.; Seo, S.; Oh, M. J.; Lee, M.; Lee, W. B.; Yoo, P. J.; Cho, J. H.; Park, J.-H. Optoelectronic Synapse Based on IGZO-Alkylated Graphene Oxide Hybrid Structure. *Adv. Funct. Mater.* **2018**, *28*, 1804397.
(7) Lee, G. J.; Choi, C.; Kim, D. H.; Song, Y. M. Bioinspired Artificial Eyes: Optic Components, Digital Cameras, and Visual Prostheses. *Adv. Funct. Mater.* **2018**, *28*, 1705202.
(8) Todd, J. J.; Marois, R. Capacity Limit of Visual Short-Term Memory in Human Posterior Parietal Cortex. *Nature* **2004**, *428*, 751.
(9) Abbott, L. F.; Varela, J. A.; Sen, K.; Nelson, S. B. Synaptic Depression and Cortical Gain Control. *Science* **1997**, *275*, 221−224.
(10) Bliss, T. V. P.; Collingridge, G. L. A Synaptic Model of Memory: Long-Term Potentiation in the Hippocampus. *Nature* **1993**, *361*, 31.
(11) Atkinson, R. C.; Shiffrin, R. M. Human Memory: A Proposed System and Its Control Processes. *Psychol. Learn. Motiv.* **1968**, *2*, 89−195.
(12) Chua, L. Memristor-The Missing Circuit Element. *IEEE Trans. Circuit Theory* **1971**, *18*, 507−519.
(13) Chua, L. O.; Kang, S. M. Memristive Devices and Systems. *Proc. IEEE* **1976**, *64*, 209−223.
(14) Strukov, D. B.; Snider, G. S.; Stewart, D. R.; Williams, R. S. The Missing Memristor Found. *Nature* **2008**, *453*, 80−83.
(15) Wang, Z.; Joshi, S.; Savel'ev, S. E.; Jiang, H.; Midya, R.; Lin, P.; Hu, M.; Ge, N.; Strachan, J. P.; Li, Z.; Wu, Q.; Barnell, M.; Li, G. L.; Xin, H. L.; Williams, R. S.; Xia, Q.; Yang, J. J. Memristors with Diffusive Dynamics as Synaptic Emulators for Neuromorphic Computing. *Nat. Mater.* **2017**, *16*, 101−108.
(16) Yang, J. J.; Strukov, D. B.; Stewart, D. R. Memristive Devices for Computing. *Nat. Nanotechnol.* **2013**, *8*, 13−24.
(17) Kim, S. G.; Han, J. S.; Kim, H.; Kim, S. Y.; Jang, H. W. Recent Advances in Memristive Materials for Artificial Synapses. *Adv. Mater. Technol.* **2018**, *3*, 1800457.
(18) Yoon, C.; Lee, J. H.; Lee, S.; Jeon, J. H.; Jang, J. T.; Kim, D. H.; Kim, Y. H.; Park, B. H. Synaptic Plasticity Selectively Activated by Polarization-Dependent Energy-Efficient Ion Migration in an Ultrathin Ferroelectric Tunnel Junction. *Nano Lett.* **2017**, *17*, 1949−1955.
(19) Shi, Y.; Liang, X.; Yuan, B.; Chen, V.; Li, H.; Hui, F.; Yu, Z.; Yuan, F.; Pop, E.; Wong, H. S. P.; Lanza, M. Electronic Synapses Made of Layered Two-Dimensional Materials. *Nat. Electron.* **2018**, *1*, 458−465.
(20) Wang, Y.; Zhang, Z.; Xu, M.; Yang, Y.; Ma, M.; Li, H.; Pei, J.; Shi, L. Self-Doping Memristors with Equivalently Synaptic Ion Dynamics for Neuromorphic Computing. *ACS Appl. Mater. Interfaces* **2019**, *11*, 24230−23240.
(21) Sangwan, V. K.; Lee, H. S.; Bergeron, H.; Balla, I.; Beck, M. E.; Chen, K. S.; Hersam, M. C. Multi-Terminal Memtransistors from Polycrystalline Monolayer Molybdenum Disulfide. *Nature* **2018**, *554*, 500−504.
(22) Chang, T.; Jo, S.-H.; Lu, W. Short-Term Memory to Long-Term Memory Transition in a Nanoscale Memristor. *ACS Nano* **2011**, *5*, 7669−7676.
(23) He, H. K.; Yang, R.; Zhou, W.; Huang, H. M.; Xiong, J.; Gan, L.; Zhai, T. Y.; Guo, X. Photonic Potentiation and Electric Habituation in Ultrathin Memristive Synapses Based on Monolayer MoS_2. *Small* **2018**, *14*, 1800079.
(24) Sangwan, V. K.; Jariwala, D.; Kim, I. S.; Chen, K. S.; Marks, T. J.; Lauhon, L. J.; Hersam, M. C. Gate-Tunable Memristive Phenomena Mediated by Grain Boundaries in Single-Layer MoS_2. *Nat. Nanotechnol.* **2015**, *10*, 403−406.
(25) Utama, M. I. B.; Kleemann, H.; Zhao, W.; Ong, C. S.; Da Jornada, F. H.; Qiu, D. Y.; Cai, H.; Li, H.; Kou, R.; Zhao, S.; Wang, S.; Watanabe, K.; Taniguchi, T.; Tongay, S.; Zettl, A.; Louie, S. G.; Wang, F. A Dielectric-Defined Lateral Heterojunction in a Monolayer Semiconductor. *Nat. Electron.* **2019**, *2*, 60.
(26) Hou, W.; Azizimanesh, A.; Sewaket, A.; Peña, T.; Watson, C.; Liu, M.; Askari, H.; Wu, S. M. Strain-Based Room-Temperature Non-Volatile $MoTe_2$ Ferroelectric Phase Change Transistor. *Nat. Nanotechnol.* **2019**, *14*, 668−673.
(27) Radisavljevic, B.; Radenovic, A.; Brivio, J.; Giacometti, V.; Kis, A. Single-Layer MoS_2 Transistors. *Nat. Nanotechnol.* **2011**, *6*, 147−150.
(28) Ovchinnikov, D.; Allain, A.; Huang, Y.-S.; Dumcenco, D.; Kis, A. Electrical Transport Properties of Single-Layer WS_2. *ACS Nano* **2014**, *8*, 8174−8181.
(29) Desai, S. B.; Madhvapathy, S. R.; Sachid, A. B.; Llinas, J. P.; Wang, Q.; Ahn, G. H.; Pitner, G.; Kim, M. J.; Bokor, J.; Hu, C.; Wong, H. S.; Javey, A. MoS_2 Transistors with 1-Nanometer Gate Lengths. *Science* **2016**, *354*, 99−102.
(30) Jiang, S.; Shan, J.; Mak, K. F. Electric-Field Switching of Two-Dimensional Van Der Waals Magnets. *Nat. Mater.* **2018**, *17*, 406−410.
(31) Huang, B.; Clark, G.; Klein, D. R.; MacNeill, D.; Navarro-Moratalla, E.; Seyler, K. L.; Wilson, N.; McGuire, M. A.; Cobden, D. H.; Xiao, D.; Yao, W.; Jarillo-Herrero, P.; Xu, X. Electrical Control of 2D Magnetism in Bilayer CrI_3. *Nat. Nanotechnol.* **2018**, *13*, 544−548.
(32) Ross, J. S.; Klement, P.; Jones, A. M.; Ghimire, N. J.; Yan, J.; Mandrus, D. G.; Taniguchi, T.; Watanabe, K.; Kitamura, K.; Yao, W.; Cobden, D. H.; Xu, X. Electrically Tunable Excitonic Light-Emitting Diodes Based on Monolayer WSe_2 *p-n* Junctions. *Nat. Nanotechnol.* **2014**, *9*, 268−272.

DOI: 10.1021/acsnano.9b07687
ACS Nano XXXX, XXX, XXX−XXX

(33) Lopez-Sanchez, O.; Lembke, D.; Kayci, M.; Radenovic, A.; Kis, A. Ultrasensitive Photodetectors Based on Monolayer MoS_2. *Nat. Nanotechnol.* **2013**, *8*, 497−501.
(34) Ko, C.; Lee, Y.; Chen, Y.; Suh, J.; Fu, D.; Suslu, A.; Lee, S.; Clarkson, J. D.; Choe, H. S.; Tongay, S.; Ramesh, R.; Wu, J. Ferroelectrically Gated Atomically Thin Transition-Metal Dichalcogenides as Nonvolatile Memory. *Adv. Mater.* **2016**, *28*, 2923−2930.
(35) Lipatov, A.; Li, T.; Vorobeva, N. S.; Sinitskii, A.; Gruverman, A. Nanodomain Engineering for Programmable Ferroelectric Devices. *Nano Lett.* **2019**, *19*, 3194−3198.
(36) Lipatov, A.; Sharma, P.; Gruverman, A.; Sinitskii, A. Optoelectrical Molybdenum Disulfide (MoS_2) Ferroelectric Memories. *ACS Nano* **2015**, *9*, 8089−8098.
(37) Tan, H.; Fan, Y.; Zhou, Y.; Chen, Q.; Xu, W.; Warner, J. H. Ultrathin 2D Photodetectors Utilizing Chemical Vapor Deposition Grown WS_2 with Graphene Electrodes. *ACS Nano* **2016**, *10*, 7866−7873.
(38) McManus, D.; Vranic, S.; Withers, F.; Sanchez-Romaguera, V.; Macucci, M.; Yang, H.; Sorrentino, R.; Parvez, K.; Son, S. K.; Iannaccone, G.; Kostarelos, K.; Fiori, G.; Casiraghi, C. Water-Based and Biocompatible 2D Crystal Inks for All-Inkjet-Printed Heterostructures. *Nat. Nanotechnol.* **2017**, *12*, 343−350.
(39) Desai, S. B.; Madhvapathy, S. R.; Amani, M.; Kiriya, D.; Hettick, M.; Tosun, M.; Zhou, Y.; Dubey, M.; Ager, J. W.; Chrzan, D.; Javey, A. Gold-Mediated Exfoliation of Ultralarge Optoelectronically-Perfect Monolayers. *Adv. Mater.* **2016**, *28*, 4053−4058.
(40) Velicky, M.; Donnelly, G. E.; Hendren, W. R.; McFarland, S.; Scullion, D.; DeBenedetti, W. J. I.; Correa, G. C.; Han, Y.; Wain, A. J.; Hines, M. A.; Muller, D. A.; Novoselov, K. S.; Abruna, H. D.; Bowman, R. M.; Santos, E. J. G.; Huang, F. Mechanism of Gold-Assisted Exfoliation of Centimeter-Sized Transition-Metal Dichalcogenide Monolayers. *ACS Nano* **2018**, *12*, 10463−10472.
(41) Baeumer, C.; Rogers, S. P.; Xu, R.; Martin, L. W.; Shim, M. Tunable Carrier Type and Density in Graphene/$PbZr_{0.2}Ti_{0.8}O_3$ Hybrid Structures through Ferroelectric Switching. *Nano Lett.* **2013**, *13*, 1693−1698.
(42) Lee, D.; Yang, S. M.; Kim, T. H.; Jeon, B. C.; Kim, Y. S.; Yoon, J. G.; Lee, H. N.; Baek, S. H.; Eom, C. B.; Noh, T. W. Multilevel Data Storage Memory Using Deterministic Polarization Control. *Adv. Mater.* **2012**, *24*, 402−406.
(43) Boyn, S.; Grollier, J.; Lecerf, G.; Xu, B.; Locatelli, N.; Fusil, S.; Girod, S.; Carrétéro, C.; Garcia, K.; Xavier, S. Learning through Ferroelectric Domain Dynamics in Solid-State Synapses. *Nat. Commun.* **2017**, *8*, 14736.
(44) Li, T.; Lipatov, A.; Lu, H.; Lee, H.; Lee, J. W.; Torun, E.; Wirtz, L.; Eom, C. B.; Iniguez, J.; Sinitskii, A.; Gruverman, A. Optical Control of Polarization in Ferroelectric Heterostructures. *Nat. Commun.* **2018**, *9*, 3344.
(45) Xiang, D.; Liu, T.; Xu, J.; Tan, J. Y.; Hu, Z.; Lei, B.; Zheng, Y.; Wu, J.; Neto, A. H. C.; Liu, L.; Chen, W. Two-Dimensional Multibit Optoelectronic Memory with Broadband Spectrum Distinction. *Nat. Commun.* **2018**, *9*, 2966.
(46) Furchi, M. M.; Polyushkin, D. K.; Pospischil, A.; Mueller, T. Mechanisms of Photoconductivity in Atomically Thin MoS_2. *Nano Lett.* **2014**, *14*, 6165−6170.
(47) Wang, Q.; Zhang, Q.; Zhao, X.; Zheng, Y. J.; Wang, J.; Luo, X.; Dan, J.; Zhu, R.; Liang, Q.; Zhang, L.; Wong, P. K. J.; He, X.; Huang, Y. L.; Wang, X.; Pennycook, S. J.; Eda, G.; Wee, A. T. S. High-Energy Gain Upconversion in Monolayer Tungsten Disulfide Photodetectors. *Nano Lett.* **2019**, *19*, 5595−5603.
(48) Ohno, T.; Hasegawa, T.; Tsuruoka, T.; Terabe, K.; Gimzewski, J. K.; Aono, M. Short-Term Plasticity and Long-Term Potentiation Mimicked in Single Inorganic Synapses. *Nat. Mater.* **2011**, *10*, 591−595.
(49) Rubin, D. C.; Wenzel, A. E. One Hundred Years of Forgetting: A Quantitative Description of Retention. *Psychol. Rev.* **1996**, *103*, 734−760.
(50) Wang, H.; Zhao, Q.; Ni, Z.; Li, Q.; Liu, H.; Yang, Y.; Wang, L.; Ran, Y.; Guo, Y.; Hu, W.; Liu, Y. A. Ferroelectric/Electrochemical Modulated Organic Synapse for Ultraflexible, Artificial Visual-Perception System. *Adv. Mater.* **2018**, *30*, 1803961.
(51) La Barbera, S.; Vuillaume, D.; Alibart, F. Filamentary Switching: Synaptic Plasticity through Device Volatility. *ACS Nano* **2015**, *9*, 941−949.

DOI: 10.1021/acsnano.9b07687
ACS Nano XXXX, XXX, XXX−XXX